Journal of Power Sources 195 (2010) 593–598

Contents lists available at ScienceDirect

Journal of Power Sources

journal homepage: www.elsevier.com/locate/jpowsour

Short communication

Synthesis and electrochemical characterization of amorphous Li–Fe–P–B–O cathode materials for lithium batteries

Motoshi Isono[a,b,*], Shigeto Okada[b], Jun-ichi Yamaki[b]

[a] Battery Research Div., Toyota Motor Corporation, 1200 Mishuku, Susono, Shizuoka 410-1193, Japan
[b] Institute for Materials Chemistry and Engineering, Kyushu University, 6-1 Kasuga Koen, Kasuga 816-8580, Japan

ARTICLE INFO

Article history:
Received 8 June 2009
Received in revised form 20 July 2009
Accepted 21 July 2009
Available online 29 July 2009

Keywords:
Lithium battery
Cathode
Amorphous
Polyanionic material
Redox potential

ABSTRACT

Various types of amorphous Li–Fe–P–B–O were investigated for use as a cathode material. The samples were prepared by the melt quench technique with a single roll. The samples had monotonically decreasing charge–discharge profiles peculiar to amorphous materials, and were between 76 and 119 mAh g^{-1}. The electrochemical performance of these amorphous Li–Fe–P–B–O materials improved with increasing boron ratio, improving from 85 to 119 mAh g^{-1}. Although the redox potentials of amorphous Li–Fe–P–O did not shift with changing P/Fe ratio, those of amorphous Li–Fe–P–B–O did shift with changing B/P ratio. The redox potentials of the Li–Fe–P–B–O in the ratios of 2/1/2/0, 2/1/1/1, 2/1/0.5/1.5, and 2/1/0/2 were approximately 3.1, 2.9, 2.6, and 2.2 V vs. Li/Li^+, respectively. This demonstrates that the redox potentials of amorphous polyanionic materials can be tuned by adjusting the electronegativity of the glass former, such as phosphorus and boron.

1. Introduction

Since the commercialization of lithium-ion batteries, the batteries have been utilized for energy storage in mobile electric devices [1,2]. In recent years, attention has turned to the use of batteries as a power source for hybrid electric vehicles (HEV). Large-scale batteries require safety, low-cost, long cycle-life, and high energy and power density. Iron-based polyanionic materials have been widely investigated as a next-generation cathode material due to their low-cost, low environmental impact, and thermal stability [3]. Among these, there have been some important polyanionic cathode active materials such as olivine-type $LiFePO_4$, NASICON-type $Li_3Fe_2(PO_4)_3$, and condensed phosphate $LiFeP_2O_7$ in the Li–Fe–P ternary system. At present, olivine $LiFePO_4$ has demonstrated the largest energy density amid the iron polyanionic cathodes [4]. Since 1997, published results have shown that nearly 100% of the theoretical capacity and good rate performance of the $LiFePO_4$ have been achieved by carbon coating and reduction of particle size. The three-dimensional framework of olivine is stabilized by the strong covalent bonds between oxygen and phosphorus ions into PO_4^{3-} tetrahedral polyanions. The high lithium intercalation voltages are considered to be an inductive effect of phosphorus electronegativity, thereby allowing tuning of the voltages [4–6]. Recently, many studies have given preliminary evaluations of lighter BO_3 groups, such as $LiFeBO_3$, having a higher theoretical capacity despite their lower redox potential [7,8].

On the other hand, phosphorus and boron are well-known glass network formers. Amorphous materials such as vanadium oxide and $FePO_4$ have been investigated as active materials for decades [9,10]. This class of materials usually has a three-dimensional (3D) corner-sharing matrix with a large bottleneck for Li diffusion. Sakurai and Yamaki [11] initially demonstrated the excellent rechargeability of amorphous a-V_2O_5 and a-V_2O_5–P_2O_5, which were superior to that of their crystalline counterparts. In 1990, Pistoia et al. [12] reported that amorphous LiV_3O_8 showed significantly higher capacity, better rate capability, and longer cycle-life than crystalline LiV_3O_8. In addition, an amorphous phase can be obtained through either a quick-quench method or a low-temperature wet chemical method, both of which are relatively low-cost compared to conventional high-temperature solid-state sintering of crystalline materials.

In this investigation, we synthesized amorphous polyanionic materials in the Li–Fe–P ternary and Li–Fe–P–B quaternary systems, which had similar compositions to the low-cost and low environmental impact $LiFePO_4$, $Li_3Fe_2(PO_4)_3$, and $LiFeBO_3$. The electrochemical characteristics and nano-scale microstructure of various compositions of amorphous Li–Fe–P–B–O were studied. In addition, we employed the tuning of the redox potential by changing the P/Fe ratio in the Li–Fe–P–O material and the B/P

* Corresponding author at: Battery Research Div., Toyota Motor Corporation, 1200 Mishuku, Susono, Shizuoka 410-1193, Japan. Tel.: +81 55 997 9537; fax: +81 55 997 7879.
E-mail address: isono@giga.tec.toyota.co.jp (M. Isono).

0378-7753/$ – see front matter © 2009 Elsevier B.V. All rights reserved.
doi:10.1016/j.jpowsour.2009.07.038

ratio in the Li–Fe–P–B–O material, which corresponded to a variety of electronegativities.

2. Experimental

The samples were prepared using a single-roll synthesis. In this approach, lithium hydroxide (LiOH, Kishida Chem. Co.), iron oxide (FeO, Ardrich), phosporus pentoxide (P_2O_5, Nacalai Tesque), and boron oxide (B_2O_3, Kishida Chem. Co.) were mixed as lithium, iron, phosphorus, and boron sources, respectively. The mixtures were heated at 1273–1473 K for several minutes and quenched rapidly with a Cu-based roll at a speed of 5000 rpm in an argon atmosphere. The dry materials were ground to a powder with a particle size of about 19 μm. X-ray diffraction (XRD) patterns were obtained from the samples using a RINT-2000 (Rigaku) with Cu Kα radiation.

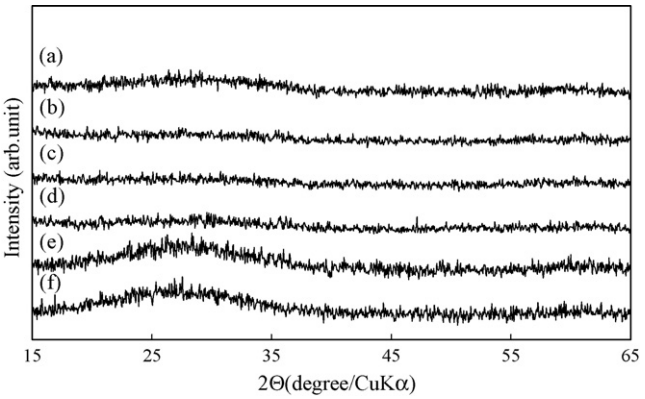

Fig. 1. XRD patterns of Li/Fe/P = (a) 1.5/1/2, (b) 2/1/2, (c) 2.5/1/2, (d) 2/1/1.5, (e) 2/1/2.5, and (f) 2/1/3.

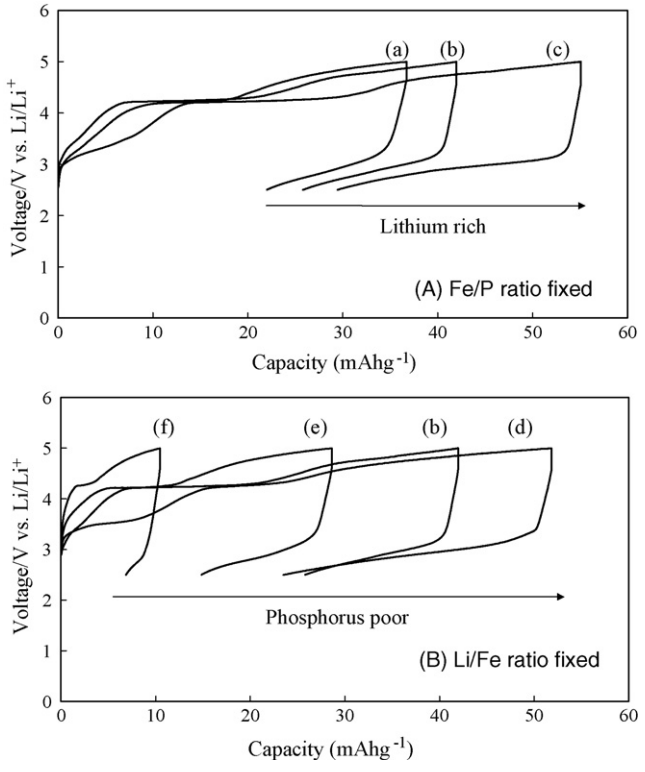

Fig. 2. Charge/discharge profiles of Li/Fe/P = (a) 1.5/1/2, (b) 2/1/2, (c) 2.5/1/2, (d) 2/1/1.5, (e) 2/1/2.5, and (f) 2/1/3.

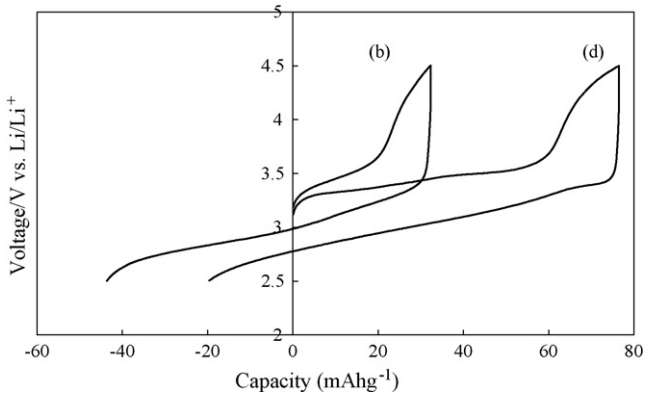

Fig. 3. Charge/discharge profiles of Li/Fe/P = (b) 2/1/2 and (d) 2/1/1.5 after planetary ball-milling.

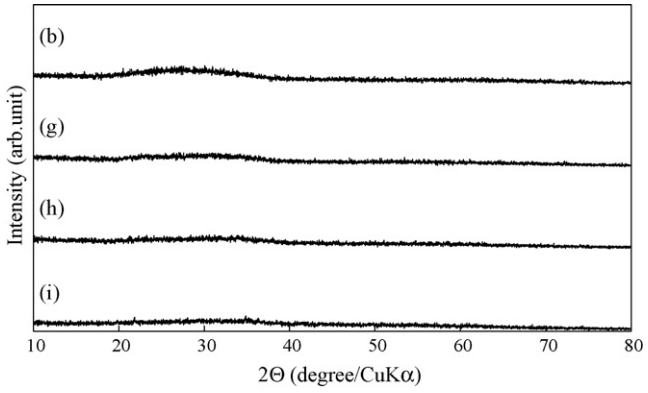

Fig. 4. XRD patterns of Li/Fe/P/B = (b) 2/1/2/0 (g) 2/1/1/1 (h) 2/1/0.5/1.5, and (i) 2/1/0/2.

Composition ratios were measured by ICP-MS (Shimazu ICPV-8100). Particle size was measured using a dynamic light-scattering particle size analyzer (Horiba LA-920).

Electrochemical characteristics of the samples were evaluated using 2032 coin-type cells using a Li metal counterelectrode. Cathode pellets were fabricated by mixing 70 wt.% active material, 25 wt.% carbon black, and 5 wt.% PTFE Teflon binder (Polyflon TFE F-103, Daikin Industry Ltd.), and then pressing (ca. 14 mg in weight and 10 mm in diameter). The obtained pellets were dried at 120 °C

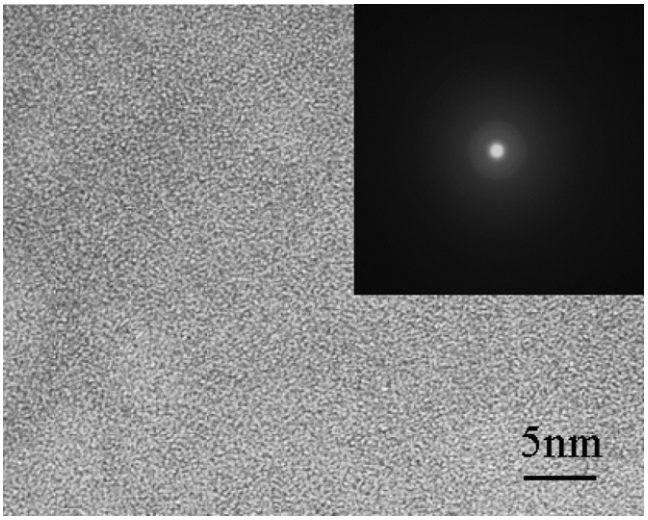

Fig. 5. TEM image and diffraction pattern of Li/Fe/P/B = (g) 2:1:1:1.

overnight. The cells were assembled in a glove box with a dew point below −70 °C. The cells were filled with a non-aqueous electrolyte (1 M $LiPF_6$/propylene carbonate (PC):ethylene carbonate (EC):dimethyl carbonate (DMC) = 1:1:3 by volume, Kishida Chem. Co.). All charge/discharge measurements (Hokuto Denko SM8) were conducted at 25 °C.

Dry ball-milling was carried out using a planetary mill (Fritsch P-7) at 300 rpm under air atmosphere. Initially, the active material was milled for 3 h. Then, the ball-milled amorphous samples and acetylene black (AB; Denki Kagaku Co. Ltd.) were milled together in a weight ratio of 70:25 for 3 h.

The morphology and nano-scale microstructure of the samples were examined using a scanning transmission electron microscope (STEM, Hitachi, HD-2000 equipped with energy dispersive X-rays (EDX)) and a transmission electron microscope (TEM, Hitachi, HF-2000).

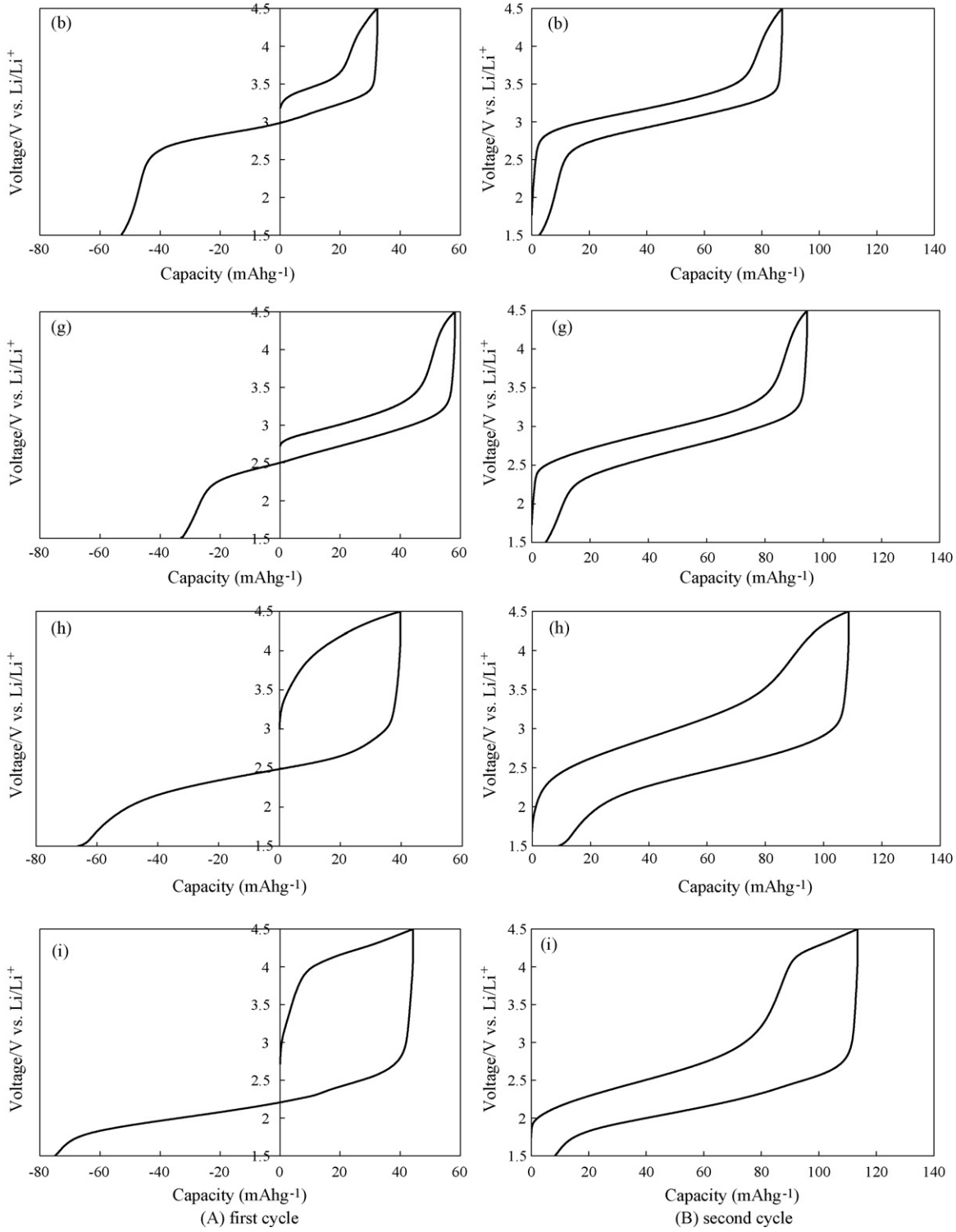

Fig. 6. Charge/discharge profiles of Li/Fe/P/B = (b) 2/1/2/0, (g) 2/1/1/1, (h) 2/1/0.5/1.5, and (i) 2/1/0/2 after planetary ball-milling.

3. Results and discussion

3.1. Li–Fe–P–O amorphous material

In this study, we selected iron as a transition metal and phosphorus as the glass network former, since olivine $LiFePO_4$ showed good electrochemical properties. A quenched Li/Fe/P = 1/1/1 sample with a composition similar to $LiFePO_4$ could not be obtained in an amorphous phase. Thus, other compositions of the Li–Fe–P–O system were investigated as amorphous cathode materials.

Fig. 1 shows XRD patterns of Li/Fe/P = (a) 1.5/1/2, (b) 2/1/2, (c) 2.5/1/2, (d) 2/1/1.5, (e) 2/1/2.5, and (f) 2/1/3. The absence of clear diffraction peaks in the patterns indicates that all samples were X-ray amorphous phases. By means of ICP-MS measurements, it was revealed that the actual Li/Fe/P atomic ratios of the samples were (a) 1.4/1.0/1.7, (b) 2.0/1.0/1.8, (c) 2.5/1.0/1.8, (d) 1.9/1.0/1.4, (e) 2.0/1.0/2.3, and (f) 1.9/1.0/2.6. This indicates that lithium and phosphorus tend to vaporize during synthesis under our preparation conditions.

The electrochemical performance of these materials was evaluated in the voltage range of 2.5–5.0 V vs. Li/Li^+ at 0.2 mA cm^{-2} charge–discharge rate, with the results presented in Fig. 2. Unfortunately, the capacities and coulombic efficiencies of these materials were considerably low, only 16–35 mAh g^{-1} and 34–55%, which may have been caused by a large polarization and an oxidative degradation of electrolyte. Although the samples showed poor electrochemical properties, a clear dependence between the composition and capacity was observed. Fig. 2(A) shows the lithium ratio dependence of the capacity. The Li/Fe/P samples ((a) 1.5/1/2, (b) 2/1/2, and (c) 2.5/1/2) provided reversible capacities (15, 16, and 26 mAh g^{-1}, respectively) and increasing the lithium ratio improved the electrochemical properties. Fig. 2(B) shows the phosphorus ratio dependence of the capacity. The capacities of Li/Fe/P = (d) 2/1/1.5, (b) 2/1/2, (e) 2/1/2.5, and (f) 2/1/3 samples were 28, 16, 14, and 4 mAh g^{-1}, respectively. This indicates that the capacity increased with decreasing phosphorus ratio. In other words, a high lithium and low phosphorus ratio improved the electrochemical properties of these materials. The reason for the observed results is not clear, but we can infer that the sample with the higher lithium ratio had a higher Li^+ diffusivity, and the sample with the lower phosphorus ratio had a higher electrical conductivity.

For improvement of the electrochemical performance, lithium transition metal phosphates require both a small particle size and a carbon coating, to improve the lithium diffusion kinetics and the intrinsic electronic conductivity, respectively. Therefore, planetary ball-milling was carried out to reduce the particle size and coat with carbon. Li/Fe/P samples having 2/1/1.5 and 2/1/2 ratios were selected to investigate the redox potential of different P/Fe ratios. Although the conditions of ball-milling were not optimized, dynamic light-scattering particle size analysis confirmed that the average particle size was reduced from approximately 19 to 3 μm.

Fig. 3 illustrates the first voltage profiles of ball-milled Li/Fe/P = (b) 2/1/2 and (d) 2/1/1.5 in the range of 2.5–4.5 V vs. Li/Li^+ at 0.2 mA cm^{-2} charge and discharge rates. The result indicated that iron oxidized during ball-milling, especially in the Li/Fe/P = (b) 2/1/2 sample, and the electrochemical properties of the carbon-coated Li–Fe–P–O with reduced particle size were significantly improved. The capacities of Li/Fe/P (b) 2/1/2 and (d) 2/1/1.5 increased from 16 and 28 to 76 and 91 mAh g^{-1}, respectively, despite the micron-sized particles. These samples had monotonically decreasing charge–discharge profiles, corresponding to amorphous materials. This proved that amorphous Li–Fe–P–O materials are electrochemically active. The redox potentials of these two samples with different P/Fe ratios were both around 3.1 V vs. Li/Li^+. The difference between the redox potentials of these samples was very small, indicating that it is difficult to tune the redox potential by variation of the P/Fe ratio. Hence, amorphous Li–Fe–P–B–O materials with various P/B ratios were thereafter explored, since the discharge voltage of $LiFeBO_3$, which has a higher theoretical capacity, is almost 1 V lower than that of $LiFePO_4$, since boron has a lower electronegativity than phosphorus [7,8].

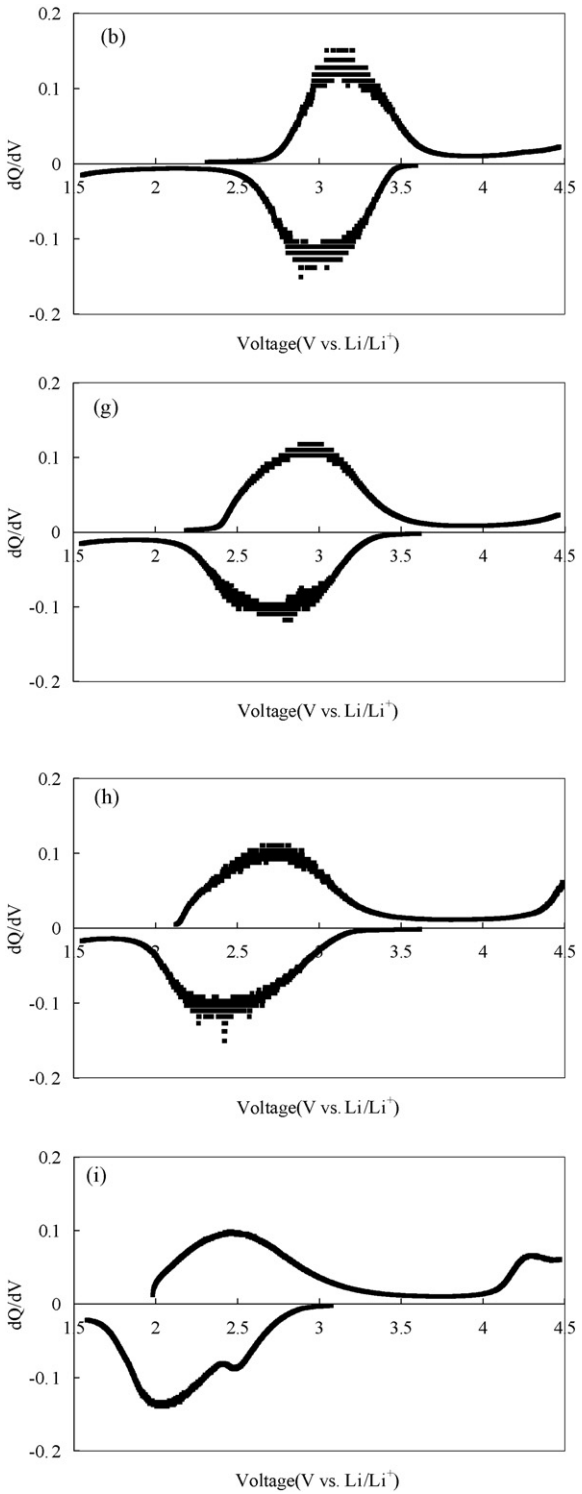

Fig. 7. dQ/dV vs. *V* plots of Li/Fe/P/B = (b) 2/1/2/0, (g) 2/1/1/1, (h) 2/1/0.5/1.5, and (i) 2/1/0/2 in the second cycle.

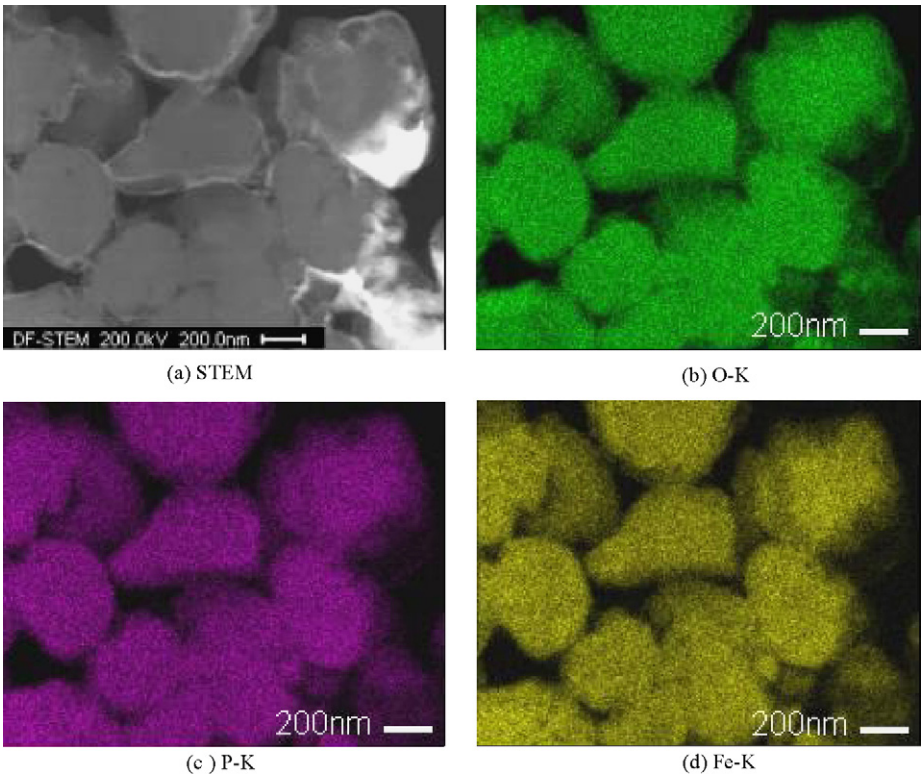

(a) STEM (b) O-K

(c) P-K (d) Fe-K

Fig. 8. STEM image and EDX mapping of O, P, and Fe for Li/Fe/P/B = (g) 2/1/1/1.

3.2. Li–Fe–P–B–O amorphous material

XRD patterns from Li/Fe/P/B = (b) 2/1/2/0, (g) 2/1/1/1, (h) 2/1/0.5/1.5, and (i) 2/1/0/2 samples are shown in Fig. 4. No diffraction peaks were observed from any matrix, suggesting that the crystal structures of these samples were X-ray amorphous phases. The actual atomic ratios of the Li/Fe/P/B samples were found to be (b) 2.0/1.0/1.8/0, (g) 1.6/1.0/0.9/0.9, (h) 1.7/1.0/0.5/1.5, and (i) 2.1/1.0/0/2.3 with ICP-MS measurements.

Fig. 5 presents a TEM image and diffraction pattern of Li/Fe/P/B = (g) 2/1/1/1, which suggest that this material was also in an amorphous phase. The TEM images and diffraction pattern of the other three samples (b, h, i) confirmed their amorphous state as well.

Fig. 6 shows the first and second charge/discharge curves of the samples under a cut-off voltage of 1.5–4.5 V vs. Li/Li^+ at a current density of 0.2 mA cm^{-2}. The reversible capacities of Li/Fe/P/B = (b) 2/1/2/0, (g) 2/1/1/1, (h) 2/1/0.5/1.5, and (i) 2/1/0/2 were 85, 91, 103, and 119 mAh g^{-1}, respectively. The sample with higher B/P ratios provided higher capacities, since boron has a lower molecular weight than phosphorous. In addition, the values of the lithium intercalation voltages qualitatively decreased with increasing B/P ratio, as expected. The electrochemical reaction of iron phosphates, such as $LiFePO_4$, $Li_3Fe_2(PO_4)_3$, and $LiFeP_2O_7$, occurred at potentials of 3.4, 2.8, and 2.9 V vs. Li/Li^+, which were close to the discharge voltage range of Li/Fe/P/B = (b) 2/1/2/0 [5]. On the other hand, the voltage of $LiFeBO_3$ was 2.3 V vs. Li/Li^+, also close to the value for Li/Fe/P/B = (i) 2/1/0/2.

Fig. 7 shows dQ/dV vs. V plots of these four samples in the second cycle to reveal the redox potential dependence of the B/P ratio. The main redox peaks (the average of oxidation and reduction potentials) of Li/Fe/P/B = (b) 2/1/2/0, (g) 2/1/1/1, (h) 2/1/0.5/1.5, and (i) 2/1/0/2 were about 3.1, 2.9, 2.6, and 2.2 V vs. Li/Li^+, respectively. Additional anodic and cathodic peaks were observed in Li/Fe/P/B = (i) 2/1/0/2 at 4.3 and 2.5 V vs. Li/Li^+, respectively. The small cathodic peak disappeared in measurements in the potential range of 1.5–3.5 V vs. Li/Li^+, and the anodic peak the disappeared at 4.3 V vs. Li/Li^+, suggesting these reactions are coupled. Although it is necessary to conduct more investigation in order to explain this phenomenon in detail, we believe that it may be due to a Fe^{3+}/Fe^{4+} redox reaction. The results indicated that the redox potential gradually decreased with an increasing B/P ratio. The absence of peak separation in Li/Fe/P/B = (g) 2/1/1/1 and (h) 2/1/0.5/1.5 samples suggests that these samples were not mixtures of Li/Fe/P/B = (b) 2/1/2/0 and (i) 2/1/0/2, but were of a uniform amorphous phase. The phase separation of these samples was verified using EDX elemental mapping.

Fig. 8 shows an STEM image and EDX mapping of oxygen, phosphorus, and iron in the Li/Fe/P/B = (g) 2/1/1/1 cathode material, and indicates that the all elements were uniformly distributed. The other three samples also had uniform distributions. Although the distribution of lithium and boron was not clear, these four samples had no phase separation. This means that the redox potential of these amorphous samples was tuned by the mixing of phosphate and boron. We are aware of no previous report of redox potential tuning via mixed X oxoanion (XO_4, XO_3; X = P, B, etc.), except for one report regarding $Li_{1+x}Fe_2(SO_4)_2(PO_4)$, because it is difficult to obtain the solid solution over a wide composition range [13]. Therefore we believe that this phenomenon will be advantageous for amorphous materials.

4. Conclusion

Cathode materials synthesized by melt quenching with single-roll, amorphous Li–Fe–P–O and Li–Fe–P–B–O materials were studied. Among the cathode materials investigated, the reversible capacities of Li/Fe/P = (b) 2/1/2 and (d) 2/1/1.5 were 76 and 91 mAh g^{-1} in the potential range of 2.5–4.5 V vs. Li/Li^+, respectively. The charge/discharge profiles indicated that these carbon-coated amorphous materials are electrochemically active

despite having micron-sized particles. These two amorphous materials had similar redox potentials, indicating that their redox potentials are not tunable by changing the P/Fe ratio.

On the other hand, the reversible capacities of Li/Fe/P/B = (b) 2/1/2/0, (g) 2/1/1/1, (h) 2/1/0.5/1.5, and (i) 2/1/0/2 were 85, 91, 103, and 119 mAh g^{-1}, respectively, over the range of 1.5–4.5 V vs. Li/Li^+. The redox potential of amorphous Li–Fe–P–B–O decreased with increasing B/P ratio, indicating that the redox potential was controlled by the electronegativity of the heteroelements in the polyanion. The tunable discharge voltage resulting from different heteroatomic ratios with various electronegativities is an advantage of amorphous polyanionic cathodes. We believe that these amorphous Li–Fe–P–B–O materials are good potential candidates for the cathode of future lithium-ion batteries.

References

[1] J.-M. Tarascon, M. Armand, Nature 414 (2001) 359–367.
[2] T. Nagaura, T. Tozawa, Prog. Batt. Sol. Cells 9 (1990) 209.
[3] K.S. Nanjundaswamy, A.K. Padhi, J.B. Goodenough, S. Okada, H. Ohtsuka, H. Arai, J. Yamaki, J. Solid State Ionics 92 (1996) 1.
[4] A.K. Padhi, K.S. Nanjundaswamy, J.B. Goodenough, J. Electrochem. Soc. 144 (1997) 1188.
[5] A.K. Padhi, K.S. Nanjundaswamy, C. Masquelier, S. Okada, J.B. Goodenough, J. Electrochem. Soc. 144 (1997) 1609.
[6] A.K. Padhi, K.S. Nanjundaswamy, C. Masqueiler, J.B. Goodenough, J. Electrochem. Soc. 144 (1997) 2581.
[7] V. Legagneur, Y. An, A. Mosbah, R. Portal, A. Le Gal La Salle, A. Verbaere, D. Guyomard, Y. Piffard, J. Solid State Ionics 139 (2001) 37.
[8] Y.Z. Dong, Y.M. Zhao, Z.D. Shi, X.N. An, P. Fu, L. Chen, Electrochim. Acta 53 (2008) 2339.
[9] S. Okada, T. Yamamoto, Y. Okazaki, J. Yamaki, M. Tokunaga, T. Nishida, J. Power Sources 146 (2005) 570.
[10] P.P. Prosini, M. Lisi, S. Scaccia, M. Carewska, F. Cardellini, M. Pasquali, J. Electrochem. Soc. 149 (2002) A297.
[11] Y. Sakurai, J. Yamaki, J. Electrochem. Soc. 132 (1985) 512.
[12] G. Pistoia, M. Pasquali, G. Wang, L. Li, J. Electrochem. Soc. 137 (1990) 820.
[13] A.K. Padhi, V. Manivannan, J.B. Goodenough, J. Electrochem. Soc. 145 (1998) 1518.